Force Equations for Festo Artificial Muscle*

Ben Bolen[1 [0000−0003−3789−7205]] and Alex Hunt[1 [0000−0002−3820−4821]]

Portland State University, Portland OR 97201, USA bbolen83@gmail.com

Abstract. Biomimetic robot joints may be articulated with various types of artificial muscles. The specific type of artificial muscle investigated in this study are the 10 mm, 20 mm and 40 mm inner diameter (ID) Festo Corporation braided pneumatic actuators (BPAs). BPAs are comparable to biological muscle in that they have force-length curves that are grossly similar to real muscles, are more energy efficient, and have a high specific power. At the same time, however, they also have limitations that need to be considered, such as their lower maximum contractile capacity and flexibility when compared to human muscles. An isometric force test stand was created to determine the steady-state force-length-pressure (FLP) relationship in 10 mm Festo BPAs. Festo data was used to construct FLP curves for the 20 mm and 40 mm ID BPAs. The first task, however, was to quantify results from actuators of different resting lengths (l_{rest}) and configurations. Testing for isometric BPA force values in these configurations allowed for the quantification of the difference between measured and expected results, as well as of the factors that were important in these differences. An equation is derived for the relationship between l_{rest} and the maximum force ($F_{max_{10}}$) of a ϕ10 mm Festo BPA such that $F_{max_{10}}(l_{rest})$. A nondimensionalized force equation is derived for each BPA ID, with each equation only requiring two variables (e.g., relative pressure P^* and relative strain) and a minimum number of coefficients. Re-dimensionalized actuator force equations are then just the maximum force value for an actuator multiplied by the nondimensionalized force equation.

Keywords: Braided Pneumatic Actuators · McKibben Actuator · Artificial Muscle · Function Fit.

1 Introduction

There are different types of biomimetic robotics. From using biological principles and behaviors as inspiration for robot design, to using artificial muscle to actuate biomimetic 3D printed skeletons. In the discipline of biomimetic robotics, high fidelity humanoid robots can help improve our understanding of both human biomechanics and the underlying neuromechanical systems that control them [10,1]. Experiments can be done with robots that would be neither practical nor

* Supported by Portland State University and NSF DBI 2015317 as part of the NSF/CIHR/DFG/FRQ/UKRI-MRC Next Generation Networks for Neuroscience Program.

ethical if done on human test subjects, and modifying robotic platforms is a potentially faster and cheaper alternative to human observation studies.

For truly biomimetic humanoid robots to go a step beyond being merely bio-inspired, it is unclear how the actuator affects other aspects of the control. One requirement for proposed artificial muscle-actuators should be that they be able to produce isometric torque about humanoid joints that meets or exceeds values measured in humans. There are several interesting methods of actuating robotic joints, including artificial muscles, electric motors (either directly driving the joints or via cable systems), or hydraulics [4,8]. Electric motors tend to be limited by magnetic saturation, heat dissipation requirements, lack of compliance, limits to power output when using mechanical gearing, and have torque curves unlike that of real muscles [11]. Hydraulic actuators have a high power/weight ratio but are generally heavy, less energy efficient than biological muscle, and require a dedicated hydraulic fluid system to operate [11]. Dielectric elastomer actuators (DEAs) are a subset of electronic-electroactive polymers (e-EAPs) and one of the most promising artificial muscles in terms of the seven performance predictive parameters compared by Liang, et al., but are limited by high voltage requirements (in the kilovolt range [7]), electromechanical instability, and requirement for compliant electrodes [6]. McKibben style braided pneumatic actuators (BPAs, also called Pneumatic Artificial Muscles or PAMs) are a promising method of actuation because they have low weight, high force/weight ratio, high efficiency, and a force-length curve that is grossly similar to actual muscle. Routing these muscles in a biomimetic arrangement can allow us to investigate and mimic the torque produced about joints by actual human muscle.

Investigating the isometric force profile of ϕ10 mm BPAs demonstrated that artificial muscles that can be made to have a similar isometric force profile to human muscle [5]. The 10 mm ID Festo BPAs have been characterized [5], but the 20 mm and 40 mm ID BPAs have not been. A more recent paper on artificial muscle attachment locations for a humanoid robot produced theoretical isometric torque curves [2]. Optimization of these muscle paths and attachment locations was done by Morrow to produce a torque curve and muscle path that match the robotic system more closely to the human biomechanical benchmark we are using [9]. These previous studies need to be combined and tested on a physical robot body. Both of these latter two papers called for 10 mm, 20 mm and 40 mm ID BPAs to be used to mimic human muscle actuators. To test the assumptions of those models, it is first necessary to reduce uncertainty by more fully characterizing the BPA FLP relationship.

Deviation from expected versus measured force in BPAs can happen in several ways. For example, Festo reports that there can be a 10% deviation from theoretical force ([3]). Kinking of the artificial muscle is also predicted to reduce the amount of available force.

We hypothesize that maximum force is a function of resting length such that $F_{max}(l_{rest})$. We further hypothesize that force, strain, and pressure can all be scaled and nondimensionalized to find a good function fit for the various

BPA diameters. These hypotheses are combined to find novel and very accurate equations for force in 10 mm, 20 mm and 40 mm ID BPAs.

2 Methods and Materials

2.1 Test Jig and BPA constructions

We built a jig to measure the isometric force F of $\phi 10$ mm BPAs with various l_{rest}, pressure (P), and strain (ϵ) values. Components of the BPA and test stand are shown in fig. 1. The test stand frame is made predominantly out of 80/20 components. The BPAs are cut to length and then they are attached to end caps with hose clamps. The endcaps are 3D printed using Onyx material on Markforged Onyx One and Mark Two printers. Onyx is a proprietary Markforged material that consists of chopped carbon fiber in nylon.

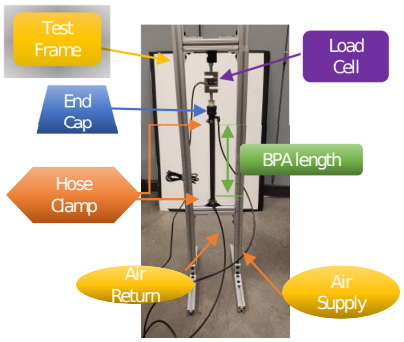

Fig. 1. A picture of a BPA in the test stand with components labeled.

2.2 Data Collection: Equipment and Procedures

Force data was collected using a CALT DYLY-103 100 kg S shaped load cell. The was load cell was used in conjunction with a HX711 Load Cell Amplifier. Pressure data comes from a Freescale MPX5700 GP 5 V pressure sensor. Building air supply pressure was controlled with two pressure regulators in series. The first is a Parker model 20R113GC 0-120 *psi* pressure regulator. The second is a Husky 3/8 in. High Performance Air Regulator HDA72200. A Festo VTUG-10-MRCR-S1T-26V20-T516LA-UL-T532S-8K valve manifold VTUG-G was used to deliver air from the pressure regulator to the actuator. This manifold is comprised of eight two-in-one bidirectional normally closed Festo VUVG-S10-T32C-AZT-M5-1T1L valves. Length measurements are performed with a FANUC tape measure.

Pressure and load cell amplifier data are sent to Matlab via an Arduino Uno style Sparkfun BlackBoard C microcontroller. The computers that used Matlab were running either Windows 10 or Windows 11. During phases when the Arduino was collecting force and pressure data to send to Matlab, the Arduino would also trigger (via Matlab) an Onsemi 2N4401 NPN transistor to make the valve manifold opened or close the valve. For other data collection the valve was manually opened and closed.

2.3 Actuator Force Calculation

BPA actuator force in our previous work has been calculated from a length-tension-pressure relationship derived by Hunt [5]. For a given robot configuration and BPA pressure P (in kPa), the scalar force F (in Newtons) for each of the artificial muscles can be determined by solving the equation:

$$P = 254\,\text{kPa} + 1.23\,\frac{\text{kPa}}{\text{N}} \cdot F + 15.6\,\text{kPa} \cdot S + 192\,\text{kPa} \cdot \tan\left(2.03\left(\frac{\epsilon}{-0.331 \times 10^{-3}\,\frac{1}{\text{N}} \cdot F + \epsilon_{max}} - 0.46\right)\right) \quad (1)$$

ϵ is the amount of contraction, and ϵ_{max} is the maximum amount of contraction in a BPA without external load that is inflated to 620 kPa. S is the hysteresis factor of the artificial muscle where $S = 1$ indicates the muscle is shortening and $S = -1$ is lengthening. For isometric contraction, set $S = 0$. An important note for (1) is that the coefficients have been updated with the correct values. We used this corrected version of the equation to create a lookup table for actuator force for a given amount of pressure and relative strain ϵ^*, defined as

$$\epsilon^* = \frac{\epsilon}{\epsilon_{max}} \quad (2)$$

With this lookup table created it is possible to use a curve fit to develop an equation for force as a function of pressure and relative strain. However, we note here two problems with the BPA characterization in [5]. The first is that this testing was done with a maximum of 111.2 N applied load, which is only about 20% of the maximum isometric force the Festo BPA is rated for at maximum pressure and no contraction. Secondly, we observed that maximum force in the BPAs decrease as the resting length decreases. Therefore, we created a test jig apparatus to test isometric force for various resting lengths of ϕ10 mm Festo BPAs at different pressures.

Each BPA resting length, l_{rest}, is measured as the distance between the hose clamps. This is how Festo defines l_{rest}, although in [5] it was measured to also include end cap length. We then inflated each BPA to maximum pressure ($P_{max} = 620\,\text{kPa}$) and measured ϵ_{max}. The BPAs were then deflated, placed vertically in the test jig made out of 80/20 pieces and fixed between two crossmembers. The force sensor was fixed between the upper crossmember and the

BPA. For 120 mm, 220 mm, 260 mm, 281 mm and 281 mm resting lengths, a Loadstar RAS1-01KS-S*C00 S Shaped load cell was used instead of the other force sensor previously mentioned. The distance between the crossmembers was adjusted to get different amounts of ϵ^*. The BPAs would then be inflated. BPAs with 120 mm, 220 mm, 260 mm, 281 mm and 281 mm resting lengths had a lot of P variation, with only 4–5 different values of ϵ^* per BPA. Conversely, BPAs with resting lengths of 112 mm, 415 mm, 455 mm, 490 mm and 518 mm had many different values of ϵ^* recorded, but all values were taken at or near P_{max}. Force and pressure data was collected as described in a previous section, above.

3 Results

Results from BPA characterization tests are shown first in fig. 2. Fig. 2**A** and fig. 2**B** shows a force response resembling an arctan curve along the resting length dimension and with a more linear response along the pressure axis. We used a surface fit to find the equation for maximum force in a $\phi 10$ mm BPA as a function of resting length and pressure, i.e. $F_{max_{10}}(l_{rest}, P)$.

$$F_{max_{10}}(l_{rest}, P) = a1 \cdot P \cdot \arctan\left(a2 \cdot P \cdot (l_{rest} - 0.0075)\right) \tag{3}$$

l_{rest} is offset by 7.5 mm because solid modeling showed our end caps contact each other at this resting length. Therefore $F_{max_{10}}(7.5\,\text{mm}) = 0$ because air would flow in one endcap and out the other (assuming perfect alignment). The curve fitting was done using the Nonlinear Least Squares method and a Least Absolute Residual robustness. $a1 = 0.4848\,\text{N}\,\text{kPa}^{-1}$ (0.4848–0.488 with 95% CI) and $a2 = 0.033\,06\,\text{kPa}^{-1}\,\text{m}^{-1}$ (0.0325–0.03362 with 95% CI). 3 has an Adjusted $R^2 = 0.9997$ and an RMSE = 2.749. Substituting $P_{max} = 620$ kPa into 3 yields the following simplified equation:

$$F_{max_{10}}(l_{rest}) = 301.6\,\text{N} \cdot \arctan\left(20.5\,\text{m}^{-1} \cdot (l_{rest} - 0.0075)\right) \tag{4}$$

Equation 4 is compared with the data in fig. 2**B**. It can be seen that $\lim_{l_{rest}\to\infty} F_{max_{10}} = 473.7\,\text{N}$. Fig. 2**C** shows an attempt at a linear fit for $\epsilon_{max}(l_{rest})$. There was a large amount of variance in the data, with the linear fit giving an adjusted $R^2 = 0.4124$ and an RMSE = 0.0083, therefore at this time we cannot say with confidence that there is a relationship between maximum strain and resting length.

As the next step in our BPA characterization, we derived an equation for normalized force in the BPA, or $F^* = F/F_{max}$. In previous work we have already used relative strain $\epsilon^* = \epsilon/\epsilon_{max}$, and here we will also introduce relative pressure $P^* = P/P_{max}$. Then we can show that $F^*(\epsilon^*, P^*)$ (fig. 3). By visualizing the lookup tables discussed above and the Festo Corporation data sheet, we can see that there appears to be an exponential relationship between ϵ^* and F, and a linear relationship between P and F. A polynomial surface fit (5th degree in ϵ^* and 1st degree in P^*) also shows an interaction between the linear P and exponential ϵ^* terms. The polynomial fit for the old data had 11 coefficients and

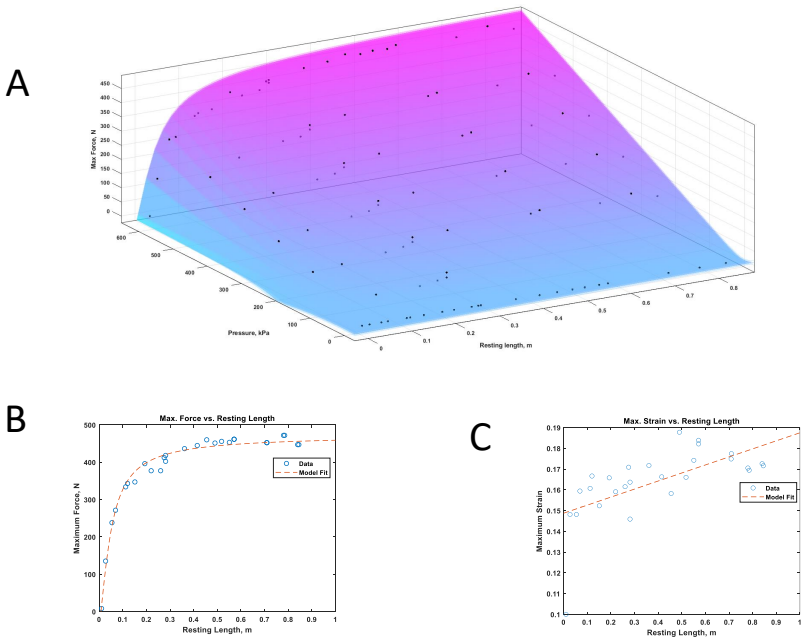

Fig. 2. Results for finding the relationship between l_{rest} and $F_{max_{10}}$, ϵ_{max}. **(A)** Surface fit for $F_{max_{10}}(l_{rest}, P)$. **(B)** $F_{max_{10}}$ versus l_{rest} at $P_{max} = 620\,\text{kPa}$. **(C)** ϵ_{max} versus l_{rest} at $P_{max} = 620\,\text{kPa}$. No conclusive relationship between ϵ_{max} and l_{rest} could be deduced from this experiment.

an adjusted $R^2 = 0.9984$. This is a good fit but it was hypothesized that we could cut the number of coefficients in half by using an equation of the form

$$F^*(\epsilon^*, P) = b0 + \exp(-b1 \cdot \epsilon^* + b2) + P \cdot \exp(-b3 \cdot \epsilon^{*2} + b4) + b5 \cdot P^* \quad (5)$$

With all the additional data collected on 10 mm ID BPAs with resting lengths given in fig. 2**B**, we then normalized the force data collected by dividing each BPA's force results by $F_{max_{10}}$ for that BPA. Pressure data was divided by P_{max}. This reduced much of the variance in the data, as shown in fig. 3, and unambiguously pointed towards using a surface fit as the right approach for F^*. Using ϵ^* and P^*, it was possible to reduce the amount of coefficients in Eq. 5 from six to only two. The equation for normalized force is

$$F^*_{10}(\epsilon^*, P^*) = -1 + \exp(-c1 \cdot \epsilon^*) + P^* \cdot \exp(-c2 \cdot \epsilon^{*2}) \quad (6)$$

with $c1 = 1.7$ (1.692–1.708 with 95% CI) and $c2 = 0.2$ (0.1968–0.2029 with 95% CI). This surface fit was done using Nonlinear Least Squares method and Least Absolute Residuals robustness. Additional data from separate tests using the 120 mm, 220 mm, 260 mm, 281 mm and 281 mm resting lengths were used for validation. Eq. 6 has an adjusted $R^2 = 0.9998$, SSE = 0.007833, and an RMSE = 0.0057. Validation SSE = 0.482595 and RMSE = 0.044292. Combining Eq. 6 and Eq. 4 will now allow researchers to determine the force F in a BPA given l_{rest}, P^*, and ϵ^*.

$$F(\epsilon^*, P^*, l_{rest}) = F^*(\epsilon^*, P^*) \cdot F_{max}(l_{rest}) \quad (7)$$

Force functions for $\phi 20$ mm and $\phi 40$ mm BPAs were also derived. Isometric force tests were not performed on these BPA sizes. Instead, values of $F_{max_{20}} = 1500$ N, $F_{max_{40}} = 6000$ N, $\epsilon_{max} = 25\%$, and $P_{max} = 600$ kPa, provided by Festo Corporation [3] were used. The normalized force equation for the $\phi 20$ mm BPA is

$$F^*_{20}(\epsilon^*, P^*) = -0.1881 + \exp(-7.965 \cdot \epsilon^* - 1.677) + P \cdot \exp(-2.036 \cdot \epsilon^{*2} - 0.1518) + 0.1518 \cdot P^* \quad (8)$$

From this equation, it appears that the coefficient $b4 = -b5$. This was confirmed with further hand tuning of the nonlinear solver. Therefore Eq. 8 has an adjusted $R^2 = 0.9985$, SSE = 0.0125, RMSE = 0.0154, and 5 coefficients. The $\phi 40$ mm BPA fit equation is

$$F^*_{40}(\epsilon^*, P^*) = -0.06974 + \exp(-8.547 \cdot \epsilon^* - 2.6287) + P^* \cdot \exp(-0.2854 \cdot \epsilon^* + 1.148) - 2.128 \cdot P^* \quad (9)$$

It can be seen that 9 is similar to the structure of Eqns. 5 and 8, but with an ϵ^* term in the second exponential instead of ϵ^{*2}. Eq. 9 has an Adjusted $R^2 = 0.9999$, SSE = 8.614×10^{-4}, and an RMSE = 0.0040.

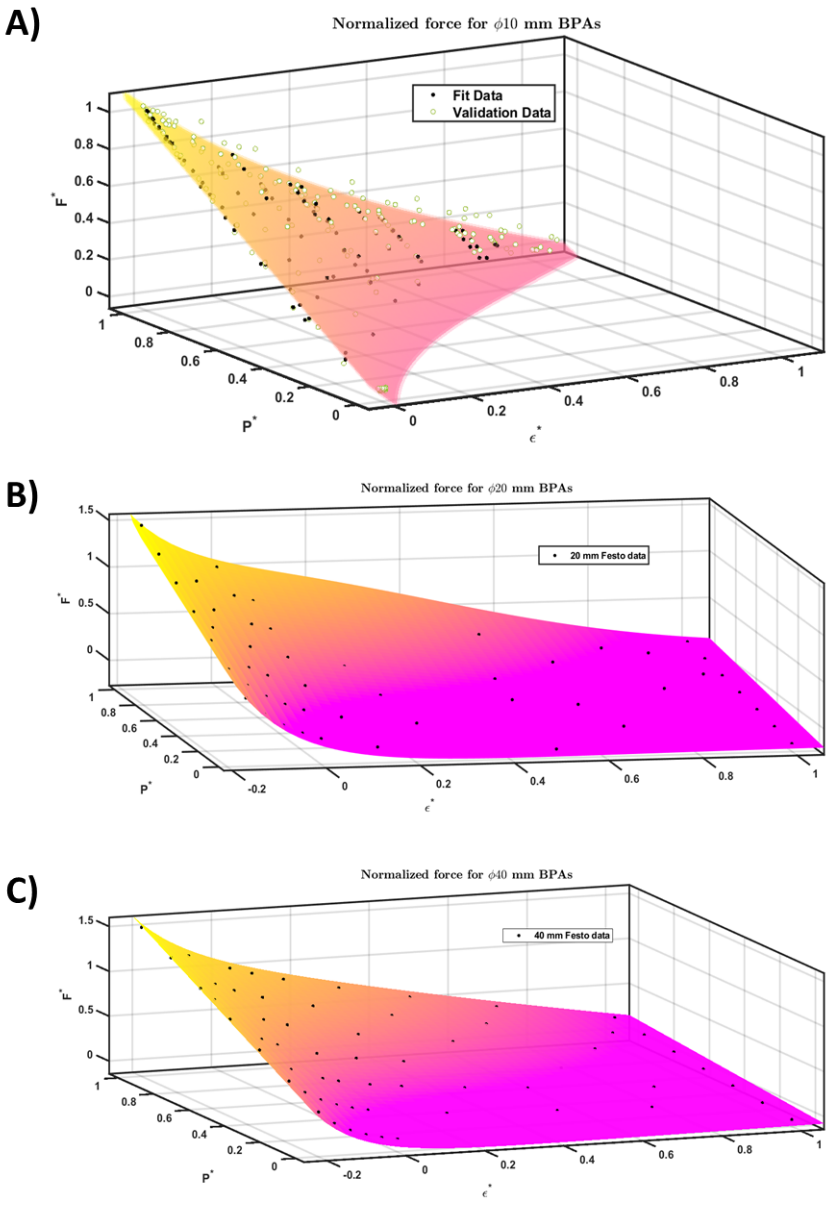

Fig. 3. Surface fit for $F^*(\epsilon^*, P^*)$ with (95% CI shown). Black circles represent fit data. **(A)**Fit data for ϕ10 mm Festo BPA. Validation data is the green circles. **(B)**Fit data for ϕ20 mm Festo BPAs. **(C)**Fit data for ϕ40 mm Festo BPAs.

4 Discussion

The analysis in this study has allowed us to create developing four novel equations for calculating force in BPAs. They are all very good fits, with three of these equations (Eqns. 4, 6, 9) having an adjusted $R^2 > 0.999$ and the other (Eq. 8) having an adjusted $R^2 > 0.998$. The equations also use a minimum amount of coefficients, with Eqns. 4, 6 using only two coefficients each, Eq. 8 having five coefficients, and Eq. 9 with six coefficients. Future work would incorporate FLP data for 20 mm and 40 mm ID BPAs, and $F_{max}(l_{rest})$ equations for these IDs as well.

Future work should also expand Eqns. 6, 8, 9 by adding a term to account for the hysteresis that occurs during BPA inflating/deflating state, similar to the $15.6\,\text{kPa} \cdot S$ term in Eq. 1. Nevertheless, Eq. 7 combines Eq. 4 and Eq. 6 to fully characterize isometric force $\phi 10$ mm Festo BPAs with a minimum amount of coefficients and variables. The work in this study will prove valuable to researchers interested in articulating bioinspired robots with pneumatic artificial muscles designed to mimic some of the characteristics of biological muscle.

Acknowledgements The authors acknowledge support by Portland State University and NSF DBI 2015317 as part of the NSF/CIHR/DFG/FRQ/UKRI-MRC Next Generation Networks for Neuroscience Program.

References

1. Asano, Y., Okada, K., Inaba, M.: Musculoskeletal design, control, and application of human mimetic humanoid Kenshiro. Bioinspiration & Biomimetics **14**(3), 036011 (Apr 2019). https://doi.org/10.1088/1748-3190/ab03fc, https://iopscience.iop.org/article/10.1088/1748-3190/ab03fc
2. Bolen, B.P., Hunt, A.J.: Determination of Artificial Muscle Placement for Biomimetic Humanoid Robot Legs. In: Martinez-Hernandez, U., Vouloutsi, V., Mura, A., Mangan, M., Asada, M., Prescott, T.J., Verschure, P.F. (eds.) Biomimetic and Biohybrid Systems, vol. 11556, pp. 15–26. Springer International Publishing, Cham (2019). https://doi.org/10.1007/978-3-030-24741-6_2, http://link.springer.com/10.1007/978-3-030-24741-6_2
3. Festo: Festo Fluidic Muscle DMSP (Apr 2022), https://www.festo.com/media/pim/556/D15000100140556.PDF
4. He, J., Gao, F.: Mechanism, Actuation, Perception, and Control of Highly Dynamic Multilegged Robots: A Review. Chinese Journal of Mechanical Engineering **33**(1), 79 (Nov 2020). https://doi.org/10.1186/s10033-020-00485-9, https://doi.org/10.1186/s10033-020-00485-9
5. Hunt, A., Graber-Tilton, A., Quinn, R.: Modeling length effects of braided pneumatic actuators. In: IDETC/CIE 2017. ASME, Cleveland, OH (Aug 2017), https://asme.pinetec.com/detc2017/data/pdfs/trk-8/DETC2017-67458.pdf
6. Liang, W., Liu, H., Wang, K., Qian, Z., Ren, L., Ren, L.: Comparative study of robotic artificial actuators and biological muscle. Advances in Mechanical Engineering **12**(6), 1687814020933409 (Jun 2020). https://doi.org/10.1177/1687814020933409, https://doi.org/10.1177/1687814020933409, publisher: SAGE Publications

7. Madden, J., Vandesteeg, N., Anquetil, P., Madden, P., Takshi, A., Pytel, R., Lafontaine, S., Wieringa, P., Hunter, I.: Artificial muscle technology: physical principles and naval prospects. IEEE Journal of Oceanic Engineering **29**(3), 706–728 (Jul 2004). https://doi.org/10.1109/JOE.2004.833135, conference Name: IEEE Journal of Oceanic Engineering
8. Mahapatra, A., Roy, S.S., Pratihar, D.K.: Multi-Legged Robots—A Review. In: Mahapatra, A., Roy, S.S., Pratihar, D.K. (eds.) Multi-body Dynamic Modeling of Multi-legged Robots, pp. 11–32. Cognitive Intelligence and Robotics, Springer, Singapore (2020). https://doi.org/10.1007/978-981-15-2953-5_2, https://doi.org/10.1007/978-981-15-2953-5_2
9. Morrow, C., Bolen, B., Hunt, A.: Optimization of Artificial Muscle Placements for a Humanoid Bipedal Robot. In: Biomimetic and Biohybrid Systems (Jul 2020)
10. Shin, H., Ikemoto, S., Hosoda, K.: Constructive understanding and reproduction of functions of gluteus medius by using a musculoskeletal walking robot. Advanced Robotics **32**(4), 202–214 (Feb 2018). https://doi.org/10.1080/01691864.2018.1434015, https://www.tandfonline.com/doi/citedby/10.1080/01691864.2018.1434015, publisher: Taylor & Francis
11. Suzumori, K., Faudzi, A.A.: Trends in hydraulic actuators and components in legged and tough robots: a review. Advanced Robotics **32**(9), 458–476 (May 2018). https://doi.org/10.1080/01691864.2018.1455606, https://doi.org/10.1080/01691864.2018.1455606, publisher: Taylor & Francis _eprint: https://doi.org/10.1080/01691864.2018.1455606